Chapter 8
Ultrafast Ionization and Fragmentation: From Small Molecules to Proteomic Analysis

Marcos Dantus and Christine L. Kalcic

Abstract Proteomic analysis offers great diagnostic relevance, because unlike DNA, different cells in an organism express different proteins. In fact, the cellular proteome can vary as a function of time or in response to stimuli. Beyond amino acid sequence, protein function depends on chemical modifications known as post-translational modifications (PTMs) that serve as "switches" and "signals" that activate or inhibit vital functions. Despite advances in mass spectrometry, which have led to the development of fully automated protein sequencing instruments, the mapping of PTMs remains a challenge. The interaction of intense near-infrared femtosecond laser pulses with isolated molecules or ions leads to the creation of radical-ion species through an ultrafast process known as tunnel ionization. The resulting unstable ions fragment according to predictable dissociation pathways. Progress analyzing and controlling the fundamental processes taking place during photoionization and fragmentation of small polyatomic molecules has led to the development of femtosecond laser-induced ionization/dissociation (fs-LID) for proteomic analysis. Fs-LID has been proven effective for the mapping of phosphorylation sites as well as other PTMs along the peptide backbone. The fundamental steps involved in fs-LID, which permits cleavage of strong bonds while leaving chemically labile bonds intact, are discussed. Numerous examples are given to illustrate this exciting new ion activation method, and potential applications are identified.

8.1 Ultrafast Field Ionization and Its Application to Analytical Chemistry

The utility of ultrafast photoionization in analytical chemistry stems from the mechanism by which energy is deposited into the population of molecules or ions being studied. While IR laser excitation is comparable to a slow-heating method, and UV laser excitation relies on resonant photon absorption, the femtosecond laser can cause ultrafast electron loss (oxidation) through a process known as tunnel ion-

M. Dantus (✉) · C.L. Kalcic
Michigan State University, East Lansing, MI, USA
e-mail: dantus@msu.edu

R. de Nalda, L. Bañares (eds.), *Ultrafast Phenomena in Molecular Sciences*, Springer Series in Chemical Physics 107, DOI 10.1007/978-3-319-02051-8_8,

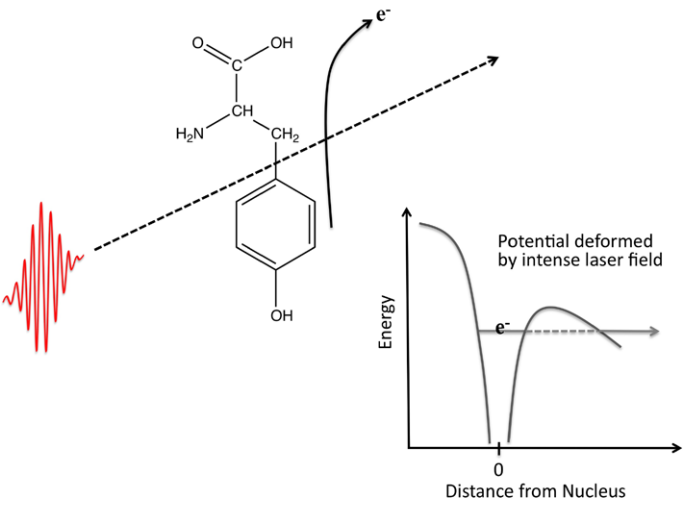

Fig. 8.1 [5] Tunnel Ionization of Tyrosine. When an ultrafast laser pulse passes by the target molecule or ion in the gas phase, the intense electric field deforms the potential felt by electrons within the molecule. As a result, the electron that is most polarizable is able to escape, leaving behind a photoionized radical site

ization [1]. Tunnel ionization is achieved when an electron, pulled by the electric field of the laser pulse, acquires sufficient energy to overcome its binding energy within a single optical cycle. This process is illustrated in Fig. 8.1. For an excitation wavelength near 800 nm, tunnel ionization requires a peak power density of 10^{14} W/cm^2 and pulse duration shorter than 35 fs. These estimates are based upon reported ionization thresholds for small molecules in an intense laser field, and have been generalized for larger molecules [2–4].

Lasers, especially those with UV and VUV wavelengths, have been used to induce bond photodissociation. Unfortunately, the most accessible chromophores present in biomolecules have a wide range of absorption maxima, as illustrated in Fig. 8.2. Therefore, wavelength tuning is typically necessary to optimize the photofragmentation process of different analytes. Unlike conventional photodissociation, tunnel ionization relies only on the presence of a polarizable electron, not a specific chromophore. In this sense, under tunneling ionization conditions, the femtosecond laser can serve as a universal excitation source.

Laser induced ionization has been a powerful method for studying the spectroscopy of weakly fluorescent molecules. When carried out with nanosecond laser pulses, ionization takes place through intermediate states that are resonant with the laser pulse energy. Given that most organic compounds have an ionization potential near 9 eV, ionization typically requires three UV photons. Such spectroscopic measurements are typically referred to as $2 + 1$ resonantly enhanced multiphoton processes (REMPI). The use of short (< 100 fs) pulses with near-IR wavelengths opens a new path for ionization that is less dependent on resonance excitation of intermediate states. The transition from multiphoton ionization (MPI) to tunneling ionization

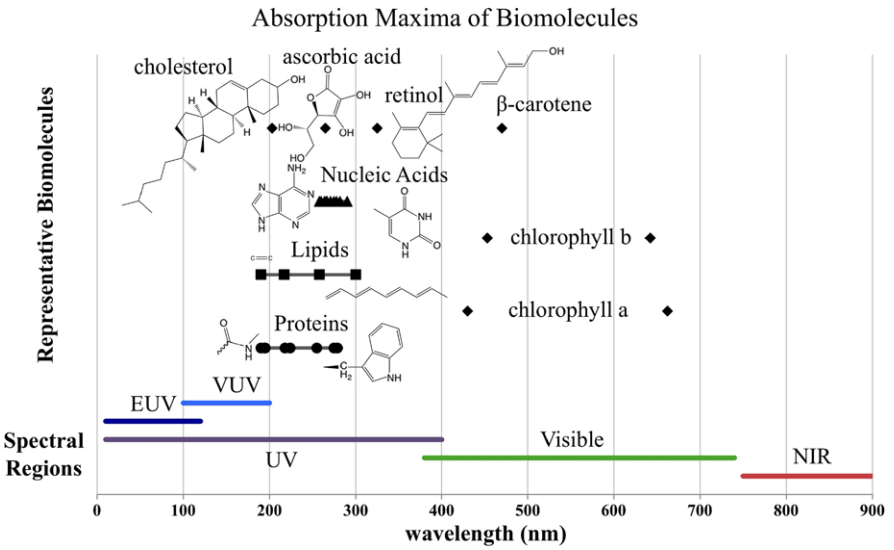

Fig. 8.2 The absorption maxima for several chromophores are plotted and grouped by classes of biomolecules. Note that larger pigments like chlorophyll have broad absorption spectra, and only the maxima are indicated in this figure

in atoms was studied by Mevel et al. who observed that distinct MPI features in the photoelectron spectra (separated by the photon energy hv) gradually disappear as tunneling ionization becomes dominant [6]. Similar work on large polyatomic molecules (benzene, naphthalene and anthracene), revealed broad featureless photoelectron spectra stretching up to 25 eV [7]. The larger the molecule, the smoother the spectrum, indicating that tunneling ionization is the dominant mechanism for above threshold ionization. The conditions of that study were 10^{13} W/cm^2, 780 nm, 170 fs. Based on those observations, the conditions of our experiments (larger molecules and much shorter pulses) place our approach in the tunneling ionization regime. Tunnel ionization is advantageous for analytical applications because it removes the need for wavelength tuning. Furthermore, as will be shown, tunnel ionization leads to ultrafast photodissociation processes that occur on a timescale faster than energy randomization. Therefore, tunnel ionization offers the ability to cleave strong bonds while leaving weaker bonds intact.

8.2 Mass Spectrometry Coupled to an Ultrafast Laser Source

8.2.1 Introduction

With the utility of soft ionization methods such as matrix-assisted laser desorption/ionization (MALDI) and electrospray ionization (ESI) which yield intact pseudomolecular ions [8, 9], tandem mass spectrometry is a robust tool for studying

molecular structure in the gas phase. The high-throughput capabilities are routinely used in the field of proteomics to efficiently analyze thousands of peptides. A typical MS/MS experiment first isolates the precursor ion population using a magnetic or electric field, and then activates this ion population to cause dissociation. The resulting product ions are recorded as the MS/MS spectrum [10]. A variety of ion activation methods can be employed, causing dissociation of the precursor ions along different pathways and leading to complementary MS/MS spectra [11]. These tandem mass spectra can be analyzed by hand or electronically using algorithms to map out the most likely structure of the original precursor ion. An ion activation method capable of breaking many different bonds within a molecule is desirable because the corresponding MS/MS spectrum will be more "information rich." In other words, it will contain a greater number of overlapping product ions that can be used to assign a more complete precursor structure with higher confidence. An ion activation method is suitable for peptide samples if it can generate sufficient product ions for unambiguous sequencing and mapping of structural modifications [12]. This structure determination can become problematic if certain regions in a peptide resist fragmentation, or if weakly bound peptide modifications dissociate preferentially to other bonds along the peptide backbone. In order to find a solution to these challenges, there is great interest in the development and characterization of new ion activation methods. Each method serves as an additional tool for tandem mass spectrometry experiments.

Given the expertise of our research group in ultrafast laser science and pulse shaping, the development of an ion activation method that utilized Femtosecond laser irradiation seemed fitting. The coupling of tandem mass spectrometry with a femtosecond laser was especially promising given developments in the field of femtosecond photoionization. In 1980, Zewail commented that the use of sufficiently short pulses would allow one to beat the timescale of energy redistribution, which typically takes place in tens of picoseconds [13]. As a result, a handful of research groups turned their focus to new experiments in laser control. The application of femtosecond lasers to study photodissociation processes in real time [14] led to the observation that bond dissociation can take place on a timescale of ~200 fs, which is two or three orders of magnitude faster than energy redistribution within a molecule. The optimization of laser fields to control chemical reactions and therefore the observed fragmentation patterns was proposed by Tannor and Rice [15]. Brumer and Shapiro realized that coherent light from the laser would cause interference between particular photochemical pathways, opening an attractive means for laser control of chemistry with nanosecond lasers [16]. The concept of creating a molecular wave packet that could be followed in time to cause selective chemistry by two or more carefully timed pulses was outlined by Rice, Kosloff and Tannor [17]. By the 1990's, scientists began to modify femtosecond laser pulses by adding linear chirp, first to control wave packet motion [18], and then to control the yield of chemical reactions [19].

The experimental work on adaptive quantum control was reviewed by Brixner and Gerber in 2003 [20]. Our group published a comprehensive review of modern (1997–2005) experimental results on coherent laser control of physicochemical processes [21]. The combination of shaped femtosecond pulses with mass spectrometry

(MS) has been hailed as the most promising technology for laser control of chemical reactions. However, despite all of the high hopes, there are only a handful of groups across the world that have conducted these types of experiments. The pioneers in this field are Gustav Gerber, who published a series of papers in 1998–2003 [22–26], Robert Levis and Hershel Rabitz [27–29], Ludger Wöste [30, 31], Thomas Weinacht [32–37], and Robert Jones [38]. All of their experiments are based on a closed-loop approach using learning algorithms to control the laser fields with feedback from the experimental signal [39]. A different strategy that has worked well on diatomic molecules is to exploit the influence of the laser field on the potential energy surfaces, through the dynamic Stark shift [40, 41]. Our group has followed a different approach, often called open-loop, in which sets of differently shaped but predefined pulses are evaluated for their ability to control chemistry [42–46].

In 2008, we published an article that reviewed the latest work in which shaped near-IR pulses were used to control molecular fragmentation [2]. In that work, we studied the laser fragmentation of 16 different molecules as a function of different phase functions, including linear chirp. We found that for several molecules the relative yield of certain fragment ions could be changed by almost two orders of magnitude. Interestingly, we found that linear chirping of the laser pulses was sufficient to cause these large changes. In those experiments, we found that vibrational coherence seemed to play a relatively small role (less than 30 % change in fragment abundance) while the pulse duration could change some fragment abundances by an order of magnitude. This observation led us to the conclusion that near-IR femtosecond laser pulses could play a very important role in the development of powerful analytical methods; however, the reproducibility of the results would depend on the implementation of methods to ensure that the pulse duration (< 40 fs) would always be the same. This goal became possible with the development of automated pulse compression by multiphoton intrapulse interference phase scan (MIIPS) [47, 48].

The combination of ultra-short intense femtosecond pulses with an ion-trap mass spectrometer led to the development of femtosecond laser-induced ionization/dissociation (fs-LID) by the Dantus and Reid groups [49]. By coupling ultrafast near-IR laser pulses with the MS^n capability of an ion trap mass spectrometer, extensive dissociation of peptides is achieved. The fs-LID instrumentation and method were first described in 2009, and the fs-LID spectra of four singly, doubly, and triply protonated peptides allowed for complete sequence determination [49]. We've found that, in positive ion mode, fs-LID is most efficient for singly protonated precursor ions, which is consistent with the estimate that ionization energy of peptides increases approximately 1.1 eV with each additional positive charge [50]. Fs-LID is also useful for the mapping of labile post-translational modifications along the peptide chain, such as phosphorylation, which was demonstrated on two synthetic phosphothreonine containing peptides. The non-ergodic dissociation patterns observed were due to the femtosecond time-scale of activation, which resulted in the ultrafast creation of a radical cation and for the ultrafast cleavage of chemical bonds faster than intramolecular energy redistribution. The applicability of fs-LID to phosphopeptide analysis was investigated further for singly protonated phosphopeptides

[51]. Radical-driven sequence ions (a, c, x, and z-ions) were observed for each phosphopeptide, and there was no dominant phosphate loss or phosphate group scrambling. The phosphorylation sites were characterized unambiguously from the fs-LID spectra [51]. Fs-LID has also been used for the analysis of protonated biomolecules other than peptides. The method works to dissociate fatty acid chains in lipids [52] and induce cross-ring cleavages in carbohydrate-based metabolites [53]. The technique was demonstrated to cleave the S–S bond in Arg^8-vasopressin, eliminating the need for wet chemistry prior to MS/MS analysis of peptides with strong disulfide bridges [54].

The most widely adopted ion activation method for MS/MS experiments is collision induced dissociation (CID), where collisions of the precursor ions with a helium bath gas causes fragmentation. As the energy gained through collisions is redistributed throughout the precursor ion, bond cleavage occurs according to bond dissociation energy. Therefore, the most abundant product ions in the MS/MS spectrum are those formed through the cleavage of the most labile bond or bonds in the analyte. For peptides, the amino acid composition greatly influences the observed dissociation pattern by affecting the amenability of the molecule to protonation, the most likely protonation sites, and proton mobility in the gas phase. These factors can influence the observed dissociation patterns by enhancing cleavage of specific bonds [55, 56]. For example, under mobile proton conditions, the backbone heteroatoms become protonated, making the peptide bonds labile [57]. This makes CID MS/MS spectra ideal for peptide sequencing when mobile protons are present, as a distribution of peptide bonds between each amino acid along the backbone chain dissociate. The mass-to-charge ratio of neighboring product ions in the MS/MS spectrum will differ by the mass of a single amino acid residue, allowing for reconstruction of the original sequence one amino acid at a time. However, this procedure is interrupted when unusually labile or non-labile bonds interfere with the standard dissociation patterns. Under non-mobile proton conditions, the proton or protons are typically sequestered at basic residues, reducing the observed sequence coverage by CID [58]. Another obstacle to sequencing are non-labile disulfide bonds between cysteine residues because they give some peptides a cyclic structure. In these cases, a single peptide bond cleavages fails to fragment the ion, as the two pieces remain linked at the disulfide bridge and the product is detected at the same m/z value as the precursor ion. For this reason, peptide samples known to contain S–S bonds are often chemically reduced prior to MS/MS analysis by CID [59]. While this retains complete or nearly complete sequence coverage, important structural information related to sulfur-sulfur connectivity in the native structure is lost. The presence of a labile chemical modification can interfere with peptide sequencing in a different manner. For example, during post-translational processing, a protein may become phosphorylated as part of a cell signaling regulation pathway. Under partially or non-mobile proton conditions, the covalent bond between the phosphate group and the amino acid side chain is more labile than the backbone peptide bonds. The H-bonding character of the phosphate group promotes proton transfer from basic side chains, leading to a charge-directed loss of H_3PO_4 [60]. This explains why, upon activation by CID, the phosphate group or groups are cleaved more readily than the

peptide backbone, and the dominant product ion reflects only this phosphoric acid loss, rather than a series of product ions containing sequence information. Phosphate group loss and position scrambling have been identified as being problematic in CID-MS^n studies [61].

The branch of proteomics that focuses on post-translational modification (PTM) analysis frequently deals with these more "problematic" samples, where comprehensive structural analysis requires cleaving strong bonds while leaving more labile bonds intact. A number of alternative ion activation methods have been introduced to achieve this required non-thermal fragmentation. Electron capture dissociation (ECD) [62] and electron transfer dissociation (ETD) [63, 64] activate the precursor ions through the formation of an unstable radical. The subsequent radical-directed fragmentation pathways are complementary to CID, and leave weakly bound PTMs intact. Photodissociation of trapped peptides in the ultraviolet [65–69] and vacuum ultraviolet [68, 70–74] regimes also generates MS/MS spectra that are similar to ETD and ECD spectra, and rely on photon absorption for ion activation rather than electron transfer [74, 75].

Fs-LID is a viable alternative to these non-statistical ion activation methods. Fs-LID differs from other laser-induced activation methods in that the laser is in the near IR region, far from the electronic excitation transitions of peptides. The ion activation is achieved through tunnel ionization, as discussed earlier. Upon ionization of a protonated peptide, the oxidized species formed is a distonic cation $[M + H]^+ \rightarrow [M + H]^{2+\bullet}$, which is susceptible to both proton- and radical-directed fragmentation pathways. As a result, fs-LID MS/MS spectra are often more information rich than CID spectra. While conservative predictions may expect product ion cleavages to occur at or near the original site of radical formation, reactive radicals have actually been demonstrated to migrate upon formation within a peptide cation. This means that the radical is mobile and that its migration is coupled with rearrangements within the molecule [76]. This can give rise to backbone cleavages and side chain losses that propagate several residues away from the initial radical site [77, 78]. This mechanism for ion activation is applicable to positive-mode MS/MS analysis of protonated peptides in any charge state and does not require a chromophore. Fs-LID is compatible with any ion trap mass spectrometer, and the interfacing of the laser can be done without compromising CID capability. Currently, the amplified laser is setup on a large optical table, but as ultrafast technology improves, the size and cost of these laser systems will decrease, making them more appealing. Ultimately, a compact femtosecond fiber laser could be brought into an existing mass spectrometry facility to make fs-LID an option for routine MS/MS analyses. Novel approaches to fiber laser design, for example self-similar evolution [79], has allowed for the development of compact fiber oscillators delivering peak power levels of 250 kW and 42 fs pulse duration [80].

Photofragmentation studies of biomolecules using UV radiation from nanosecond lasers led to the suggestion that the use of tunable fs-UV laser pulses might lead to efficient and non-ergodic dissociation of large molecules [81]. However, limited work has paired a femtosecond Ti:Sapphire laser with an ion trap mass spectrometer for such dissociation studies. Laarman et al. used a learning algorithm with pulse

shaping methods to optimize the cleavage of an acyl-N bond in Ac-Phe-NHMe to demonstrate the application of femtosecond pulse photodissociation for peptide sequencing [82]. Guyon et al. performed femtosecond pump-probe experiments on flavin, using the frequency doubled laser at 405 nm for resonant excitation of the inherent flavin chromophore [83]. Other experiments have interrogated the dissociation pathways of protonated aromatic amino acids and dipeptides using femtosecond pulses at 266 nm [84, 85]. Our work builds upon these previous experiments, but avoids the need for resonant excitation in the UV.

8.2.2 Experimental Methods

Fs-TOF Experiments on small neutral molecules were carried out using a regeneratively amplified Ti:Al_2O_3 laser seeded with a broad-band Ti:Al_2O_3 oscillator. The output was centered at 800 nm with the maximum pulse energy of 0.8 mJ. The bandwidth was ~28 nm (FWHM) resulting in ~35 fs (FWHM) transform-limited (TL) pulses. A MIIPS enabled pulse shaper [48] was placed before the amplifier to eliminate phase distortions from the laser and any optics in the setup, and to deliver arbitrary phases precisely at the target. Para-nitrotoluene (Aldrich > 99 %) was used without further purification. The fs-TOF experiments were carried out using a time-of-flight mass spectrometer (TOFMS) with a 0.5 meter field-free drift region (Fig. 8.3). Sample molecules were effused through an inlet valve into the chamber, where the pressure was maintained with a three stage differentially pumped system at 10^{-7} Torr with operational flexibility up to 10^{-5} Torr during experiments. Pulses with a 1 kHz repetition rate were focused by a 50 mm lens into the chamber to cause ionization and fragmentation of the molecules. The energy per pulse was attenuated to 100 μJ to reach a corresponding peak power density of 4.0×10^{15} W/cm^2.

Fs-LID of Trapped Ions Experiments on biomolecules were conducted by using a custom-built Quantronix (East Setauket, NY) Integra-HE amplified Ti:Al_2O_3 laser system. The broadband output of the Ti-Light oscillator is passed through a 128-pixel MIIPS-enabled pulse shaper (Biophotonic Solutions Inc, MI) before seeding a 2-stage amplifier. The system is capable of delivering a 3.0 W output with a repetition rate of 10 kHz. The pulse-shaper is used to measure and compensate phase distortions accumulated as the laser beam passes through optics in the setup, resulting in transform-limited (TL) pulses with a ~ 26 nm (FWHM) bandwidth and ~ 35 fs duration at the sample.

All samples were subjected to electrospray ionization for introduction into a Thermo Finnigan LCQ Deca XP Plus ion trap mass spectrometer. The LCQ was modified in-house to accommodate laser irradiation of the trapped ion samples. A ½″ diameter hole was drilled through the vacuum manifold in line with the ion trap, and a vacuum-sealed laser port was constructed with fused silica window. A 5 mm hole was drilled all the way through the ring electrode and the quartz spacers were notched accordingly to provide a clear path for the focused laser beam

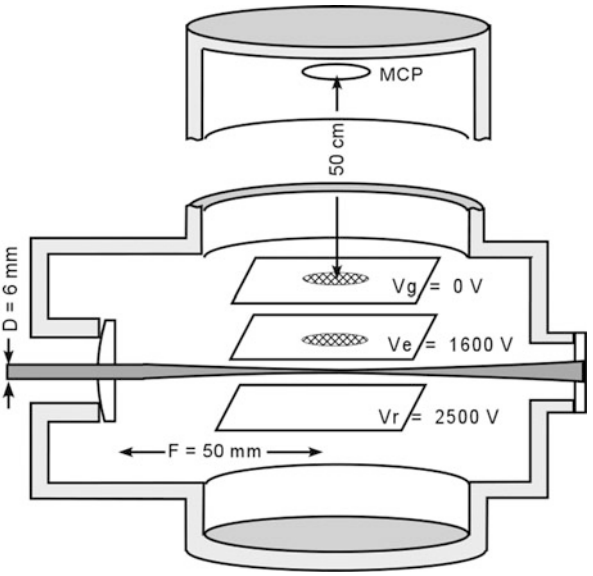

Fig. 8.3 [54] Schematic of the time-of-flight mass spectrometer. The laser beam is introduced into the chamber through a lens. Ions, generated between the repeller and extractor at high voltage, are detected by the dual microchannel plate detector after a 0.5-meter field free flying region

through the trap. Finally, a silver mirror was fixed to the vacuum manifold on the far side of the ion trap and used to direct the laser out another fused silica window in the back of the instrument. A manual flow controller was used to reoptimize the helium pressure within the trap following these structural modifications. A more detailed description of the modifications to the commercial mass spectrometer can be found elsewhere [49], and the setup is diagrammed in Fig. 8.4. The beam from the Ti-Light oscillator passes through a MIIPS Box pulse shaper equipped with a 128-pixel spatial light modulator (SLM) before seeding the amplifier. A computer is used to control the voltages across each SLM pixel, whereby the phase across the bandwidth of the laser pulse can be altered. This technology allows us to measure and compensate for phase distortions, which cleans up the laser pulses and shortens the pulse duration of the amplified system from > 70 fs to < 40 fs. The fs-LID setup utilizes this ability to ensure that the femtosecond pulses are as short as possible (transform limited) when they reach the ion packet inside the 3D ion trap. Past experiments have shown that delivering $\sim$35 fs pulses reproducibly is critical to fs-LID efficiency. The effects of dispersion, which leads to pulse broadening, severely reduces the tunnel ionization efficiency, as shown in Fig. 8.5.

The amplified laser beam is directed through a mechanical shutter, which is triggered to open and close when appropriate by the software that controls the mass spectrometer. A quarter wave plate and polarizer are used as a means of attenuating the amplified laser from the full 3.5 W output to an optimal fs-LID power. If the laser beam is too intense when it enters the vacuum manifold, the fs-LID signal-to-noise ratio suffers. This trend as a function of laser power is shown in Fig. 8.6 for a series of fs-LID spectra of protonated tryptophan. Finally, the amplified laser beam is directed up a periscope and focused through a lens before it enters the vacuum manifold via the fused silica window. Focusing the beam is necessary in order to

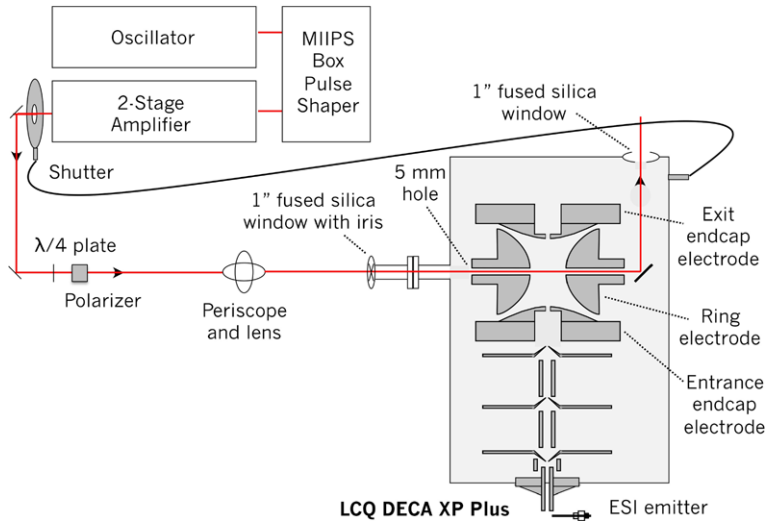

Fig. 8.4 [5] Instrumental setup of the amplified laser and 3D ion trap mass spectrometer

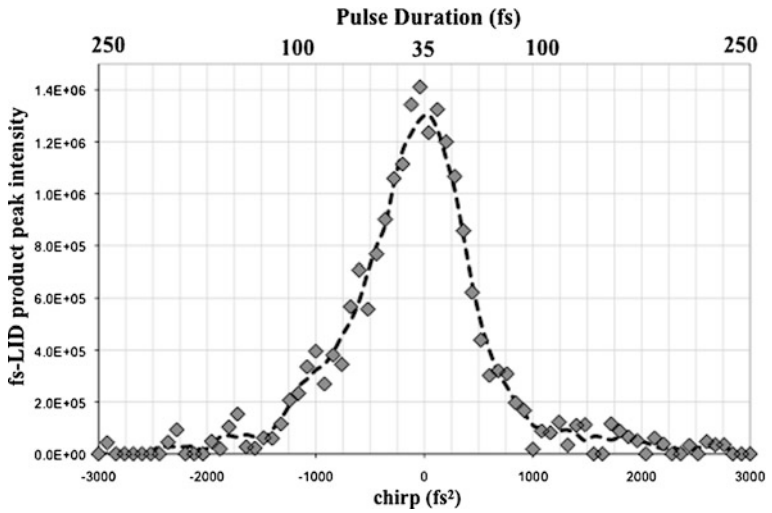

Fig. 8.5 [5] Short pulses are critical to fs-LID. Transform limited pulses with a duration of 35 fs maximize the intensity of the fs-LID product ion signal, while pulses that are stretched to 100 fs in duration result in a 80 % loss of signal intensity

pass the beam through the ion trap without hitting any of the metal surfaces, and it also provides a high peak power at the ion packet for ion activation. The unfocused beam (6.8×10^9 W/cm^2) does not provide a peak power sufficient to initiate fs-LID; experiments indicate that a peak power on the order of 10^{13} W/cm^2 must be achieved before an fs-LID product ion signal is observed (data not shown).

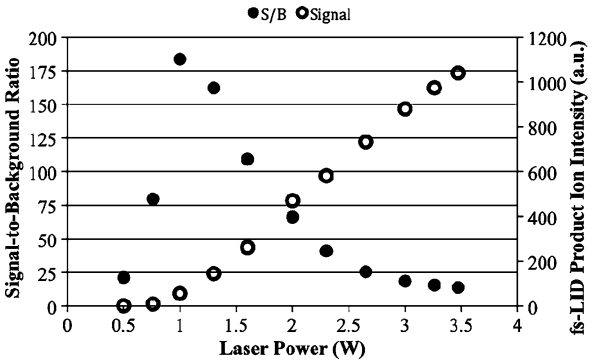

Fig. 8.6 [5] The intensity of the most abundant product ion in the fs-LID spectrum of protonated tryptophan ($[W + H]^+$) was monitored as a function of laser power (*open circles*). When the laser is allowed to irradiate a blank sample containing only MS Buffer, certain unidentified peaks are observed, most of which lie below 300 m/z (not shown). The most intense such peak observed in the $[W + H]^+$ fs-LID spectrum at 77.1 m/z was also monitored as a function of laser power. The ratio of the product ion to the 77.1 m/z ion is presented here, as the signal-to-background ratio (*closed circles*)

For these experiments, the laser was attenuated to 1.2 W (120 μJ/pulse), and focused into the ion trap using a 600 mm focal length lens, resulting in a peak laser power of 7.5×10^{13} W/cm^2. Samples were isolated using the Advanced Define Scan panel of the LCQ Tune Plus software at a q-value of 0.25. To collect fs-LID data, the normalized collision energy was set to 0 % and an activation time of 100–200 ms was used. Note that the exposure time on the shutter control box has to be manually set to match the activation time to maximize the laser-ion packet interaction without exceeding the activation window and bombarding the dynode with photons as the product ions are being ejected to generate the MS/MS spectrum. Additionally, we chose to use a 3 microscan setting and average spectra over 3–5 min for each data file.

Fs-LID data collection requires use of the built-in electronic triggering function to open and close the laser shutter during the appropriate ion activation step. To optimize our fs-LID signal before data collection, we adjust the ion trap fill time so that the isolation yields a precursor ion signal of approximately 10^6 counts. The Automatic Gain Control can be used to do this, or the fill time can be set manually. We also tweak the laser beam angle slightly off of the top periscope mirror while monitoring the photoionization product ion peak using the manual tune window. When this peak is maximized, we know we are getting the maximum laser-ion packet overlap and therefore see the best fs-LID efficiency. This slight steering of the mirror is only necessary when switching between samples that differ significantly (> 100 Da) in mass-to-charge ratio. This is likely because the ion packets are different sizes or the ion trajectories shift for precursor ions of different masses. Finally, note that fs-LID is a non-resonant ion activation method, so no wavelength tuning is necessary, nor do we modify our samples with chromophores.

8.3 Results from Small Polyatomic Molecules

8.3.1 Vibrational and Electronic Coherence

For over three decades short pulses have been used to create coherent superpositions of states and to observe quantum beats as a function of time delay. As shorter laser pulses have become available, it has become possible to create these vibrational wave packets involving vibrational modes of even the lightest atoms. Shorter pulses have also accessed the creation of superpositions of electronic states. When the vibrational or electronic wave packets are formed through excitation using a field that is one-photon resonant with the states, the formation and time evolution are well understood. Here, however, we focus on an application involving femtosecond lasers that are in the near-IR, and therefore not resonant with the dissociative or ionic states of the molecules being studied. If a typical organic molecule has an ionization-energy of 9 eV and the photon energy is ~1.5 eV, then at least 6 photons are needed to create the ion and several more are required to yield fragment ions. The focus of this section is to provide information about the vibrational and electronic coherence in small polyatomic molecules soon after they have been subjected to strong-field ionization by a near-IR femtosecond laser pulse. The extent of vibrational and electronic coherence that survives the strong-field ionization is relevant because it can be harvested in order to achieve coherent control using shaped pulses.

Strong field experiments in diatomic molecules have revealed that it is possible to form coherent vibrational and rotational wave packets. An example of such observations is the strong field ionization of deuterium to form D_2^+, and the observation of vibrational oscillations (~ 25 fs period) and rotational recurrences (~550 fs) [86, 87]. The vibrational oscillations were clearly visible when 12 fs pulses were used; however, when longer pulses were used the vibrational oscillations were no longer observed. More recently, the creation of superpositions of electronic and vibrational states has been observed following tunnel ionization of N_2, O_2, and CO with few-cycle pulses [88]. Results from the strong field ionization of CH_2I_2 show evidence of I–C–I bending coherent wave packet motion considered to arise through the formation of "multihole" wave packets. Interest in using tunnel ionization as a method for activating macromolecules being studied by mass spectrometry requires us to consider if vibrational and electronic coherence survive in larger molecules. Results from acetophenone and substituted acetophenones from our group showed evidence of coherent wave packet motion [89]. Of particular interest in that research was the effect of substituents in the aromatic ring. For example, Fig. 8.7 shows portions of the transients obtained for acetophenone (red) partially deuterated (CD_3) acetophenone (black), ortho (cyan), meta (indigo) and para (green)-methyl acetophenone. Ortho substitution increases the oscillation period from 0.7 ps to 1 ps, while meta substitution results in no oscillations. while meta substitution results in no oscillations. The observations are related to the preferred electronic configuration of the differently substituted compounds and the torsion of the carbonyl group.

Although it is suspected that the tunnel ionization process is capable of producing superpositions of electronic states, the evolution of the electronic wave packets

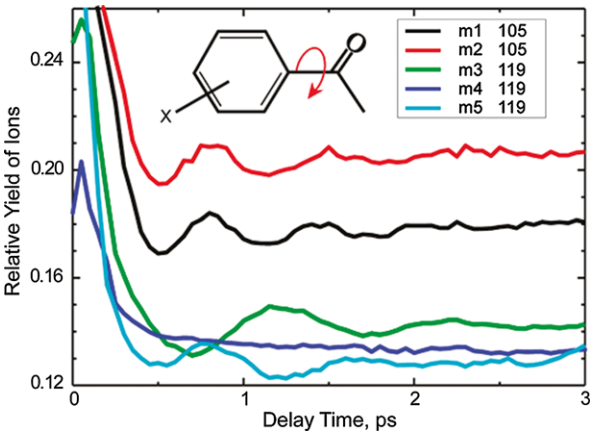

Fig. 8.7 [89] Transients obtained from acetophenone and methyl-acetophenone as a function of time delay between the pump (200 fs, 800 nm, chirped) and probe (35 fs, 800 nm, TL) pulses. Molecules are m1, acetophenone; m2, d-acetophenone; m3, 2-methyl-acetophenone; m4, 3-methyl-acetophenone; m5, 4-methyl-acetophenone. A schematic of the torsional vibration of the phenyl ring, which is thought to be responsible for the ion yield modulation, is shown

have not been observed. Electronic coherence is of particular importance because, at high energies, it could be used to control among various dissociation processes. Our group has been searching for evidence of electronic coherence following tunnel ionization of large organic molecules. Our early results indicated that the electronic coherence, if formed, was decaying within the pulse duration (∼35 fs). More recently we have found a method to detect electronic coherence following tunnel ionization. We are exploring cases in which the initial electronic coherence involves excited states in the neutral molecule and one case in which the electronic state involves the molecular ion (data not shown here). The coherence lasts for at least 100 fs and opens the window for coherent control experiments that will show large differences as a response to small differences in phase. It is becoming clear that the use of ultrashort intense pulses, lasting less than 5 optical cycles in duration, facilitates the creation of ions that exhibit coherent dynamics dictated by the coherent superposition of electronic and vibrational states. This observation has now been tested by our group with molecules with greater than 15 atoms, and we believe it will be correct for even larger molecules. The ability to create these initial coherent superpositions should allow coherent control of the fragmentation processes that is well beyond what could be achieved in the early experiments in the field involving pulse durations exceeding 50 fs.

8.3.2 Effect of Pulse Shaping

At the level of power density required for tunnel ionization, most of the molecules being subjected to fs-TOF are ionized/activated. Ionization saturation of most or-

ganic molecules is experimentally observed around 1–2 $\times$ 10^{14} W/cm^2 [3, 90]. Additionally, it was observed that shaping of the femtosecond laser pulses resulted in different product ion distributions, sparking several studies in laser control of molecular fragmentation [22]. Our group has reviewed these studies and followed up with a systematic evaluation of which field parameters are responsible for the changes observed in the fragmentation pathways [2]. We observed that the mass spectrum observed for polyatomic molecules under near-threshold ionization by transform limited sub-40 fs pulses was very similar to that obtained by electron-impact ionization (EIMS). In general, mechanisms for fragmentation following EIMS are well understood as radical-cation chemical reactions that proceed in the absence of molecular coherence. In order to better understand the system, the interaction of near-IR femtosecond laser pulses with small isolated molecules and cations was investigated through fs-TOF and fs-LID experiments on para-nitrotoluene (pNT) [54]. The different fragmentation pathways for the neutral and protonated forms of pNT were of particular interest.

Mass spectra of pNT obtained by electron ionization (EI), fs-TOF, CID, and fs-LID are shown in Fig. 8.8. The EI spectrum is obtained from the NIST database. Transform limited pulses with 35 fs time duration are used for fs-TOF and fs-LID experiments, with the peak power density of 4.0 $\times$ 10^{15} W/cm^2 and 1.6 $\times$ 10^{14} W/cm^2, respectively.

The photochemistry of pNT has been studied intensively. Although some controversy remains, the major pathways of dissociation are well established and are adopted here to explain our data. In the fs-TOF experiments, pNT molecules are tunnel ionized instantaneously. The molecular ions undergo isomerization of CH_3-f-NO_2 to CH_3-f-O-NO, as observed by the CH_3-f-O^+ product ion and the competitive production of NO_2 and NO through a common transition state [91]. In the presence of a strong field, the elimination of NO_2 is the predominant step following isomerization. The resulting $C_7H_7^+$ ions exist as an equilibrium of benzyl and tropylium ions, which was confirmed by their absorption bands at 263 and 353 nm respectively [92]. Sequential absorption of photons releases C_2H_2 fragments, giving rise to $C_5H_5^+$, $C_3H_3^+$, and C^+ ions.

The fragmentation pattern of pNT by electron ionization (Fig. 8.8) is very similar to that seen by fs-TOF with transform limited pulses. However, less molecular ion and more small fragments (C^+, H^+) are observed in the fs-TOF spectrum. This is due to the absorption of additional photons by larger fragments including molecular ions, resulting in sequential fragmentation

The fs-LID ion trap experiments on protonated pNT reveal that the even-electron, protonated molecule (MH^+) follows a slightly different fragmentation pathway than the ionized neutral ($M^{+\bullet}$). The fs-LID spectrum (Fig. 8.8) shows a combination of even- and odd-electron product ions, and is dominated by losses of heteroatoms from the nitro group. While the peak at 121 ($C_7H_7NO^{+\bullet}$), resulting from the loss of OH, is absent in the fs-TOF spectrum, all other fs-LID product ions match up with fs-TOF product ions, with an occasional shift of 1 m/z due to the retention of an extra proton. The tropylium ion is a minor product in fs-LID and therefore the benzene ring fragment ions (such as $C_5H_5^+$) are also in low abundance. While smaller

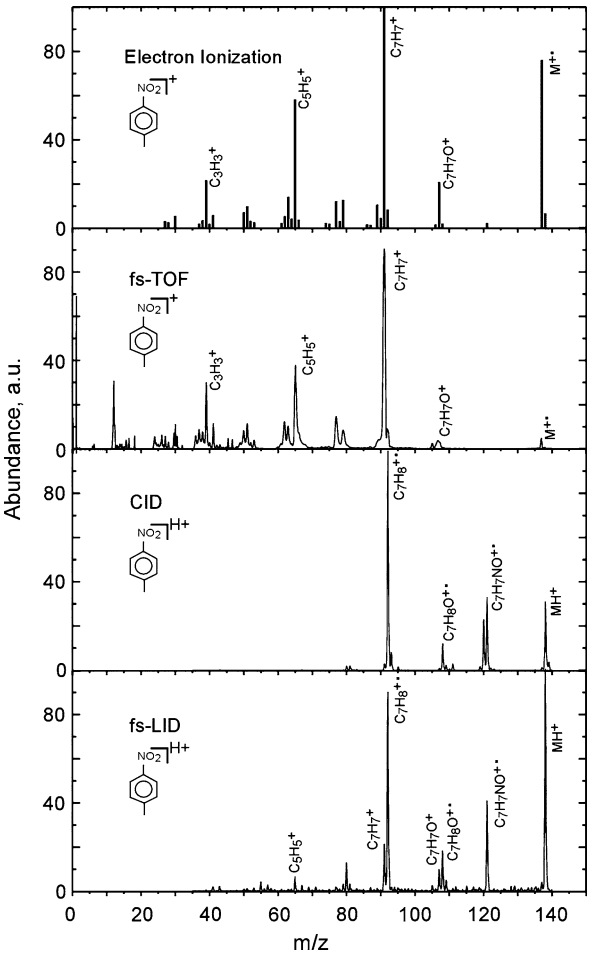

Fig. 8.8 [54] Mass spectra of para-nitrotoluene obtained by electron ionization, fs-TOF, CID, and fs-LID. Note that in the ion trap experiments (CID and fs-LID), the trapping potentials create a low mass cutoff of 35 m/z—any product ions generated below this point are ejected from the trap before the detection scan and therefore do not appear in the spectra

fragments may form upon activation with the femtosecond laser, the trapping voltages impose a low mass cutoff of 35 m/z in the ion trap; therefore, the smaller ions cannot be detected in this experiment.

While CID is a commonly employed activation method for biomolecules, it does not lead to extensive fragmentation of small organics like pNT. Nevertheless, the CID spectrum is included in Fig. 8.8 to provide an additional comparison to fs-LID. CID of pNT results in losses of OH, H_2O, NO, and NO_2. We see no tropylium ion, and therefore observe no benzene ring fragmentations. The only CID peak absent in the fs-LID spectrum corresponds to the water loss (peak 120), which comes from the protonated NO_2 group grabbing an additional proton from the benzene ring and kicking out a water molecule, leaving $C_7H_6NO^+$. This product ion provides no additional structural information.

Mass spectra of pNT were recorded as a function of linear chirp in the femtosecond laser pulses. A constant pulse energy was maintained so that larger linear chirp

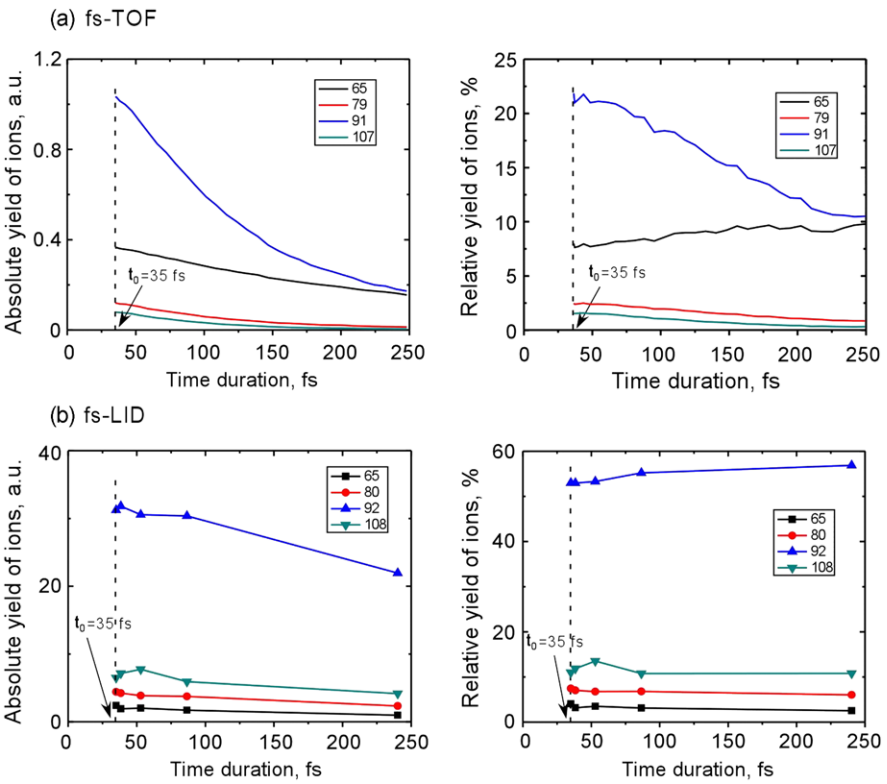

Fig. 8.9 [54] Chirp dependence of pNT fragmentation obtained by fs-TOF (panel **a**) and fs-LID (panel **b**). Absolute and relative yields of several major product ions are plotted as a function of the time duration

values result in longer pulses with lower peak intensity. The absolute and relative yields of several major product ions are plotted as a function of pulse duration in Fig. 8.9.

In the fs-TOF experiments, absolute yields of all product ions decrease with increasing pulse duration. For longer pulses, the volume in which the power density is higher than the ionization threshold is smaller, thus fewer molecules are ionized/activated and fragmented. On the other hand, the relative yields of larger fragments decrease while those of smaller fragments increase with pulse duration. This can be explained by the longer pulses giving ions more time to absorb additional photons and dissociate into smaller product ions.

Unlike the fs-TOF dependence on chirp, the fs-LID experiments show that TL pulses are ideal for ion activation in an ion trap. Longer chirped pulses result in a loss of overall fs-LID signal, with all product ion intensities decreasing uniformly (as seen by the constant relative yields in Fig. 8.9b). The difference between the TOF and ion trap data may be attributed to the different vacuum regimes utilized in each. Fragment ions are formed in the TOF-MS at 10^{-5} Torr and can continue to

dissociate into smaller and smaller pieces; however, a helium bath gas maintains a pressure around 1 mTorr in the ion trap, so as product ions are formed, they undergo collisional cooling and are stored until the detection period.

While it was known that pulse shaping led to changes in the relative yields of different fragments, it was yet to be determined if these changes were related to coherently controlled quantum mechanical interference or if they were related to ladder-switching mechanisms that were first identified when picosecond pulses were compared with nanosecond pulses. In other words, longer pulses can be absorbed by the molecule at different times, and thereby access different pathways.

In order to explore evidence of coherence in the fragmentation of p-NT using shaped laser pulses we first determined that laser intensity and central wavelength has little or no effect on the relative ion yields. We then evaluated the relative yield of several ions as a function of different families of shaped pulses (sinusoidal function, chirp, binary phases, cubic phases, etc.). The results from thousands of experiments were analyzed and there seemed to be no evidence of a vibrational or electronic coherence that had been selectively excited by one of the different shaped pulses. A selection of those results is shown in Fig. 8.10, where results are compared for four different types of shaped pulses and four different laser intensities. Note that the relative yields of $C_7H_7^+$ and $C_3H_3^+$, track closely, and show no intensity dependence.

When the study was submitted for publication the reviewer asked if p-NT was a particularly different molecule, and perhaps an exception. We then studied 16 other molecules, and our findings are best summarized in Fig. 8.11. The yield of the strongest peaks in the mass spectrum of the different molecules was tracked as a function of pulse shaping. Results are shown as a function of chirp (continuous line) and as a function of sinusoidal shaping (dotted lines). Correlation between chirp and sinusoidal shaping was achieved by matching the integrated (all masses) ion yield produced by the laser pulses. The close agreement shown in the data, evidenced as coincidence between chirped and sinusoidal shaped pulses, suggests to us that the spectral-temporal details of the pulse were not as important as the average duration of the pulses.

We concluded that pulse duration, in fact, was the most important predictor of fragmentation. One explanation for the observed effect on pulse duration is that ions are able to undergo further fragmentation through the absorption of additional photons of the incident field. Deviations from this conclusion are possible, especially when vibrational and electronic coherence survive the initial tunnel ionization process. We believe that coherent control of photofragmentation under tunnel ionization conditions should be possible, provided the excitation fields used are shorter than ~ 5 optical cycles.

8.4 Results from Peptides [5]

Here we analyze the fragmentation mechanism involved in fs-LID MS/MS of trapped peptides. We start with the protonated amino acids and several derivatives

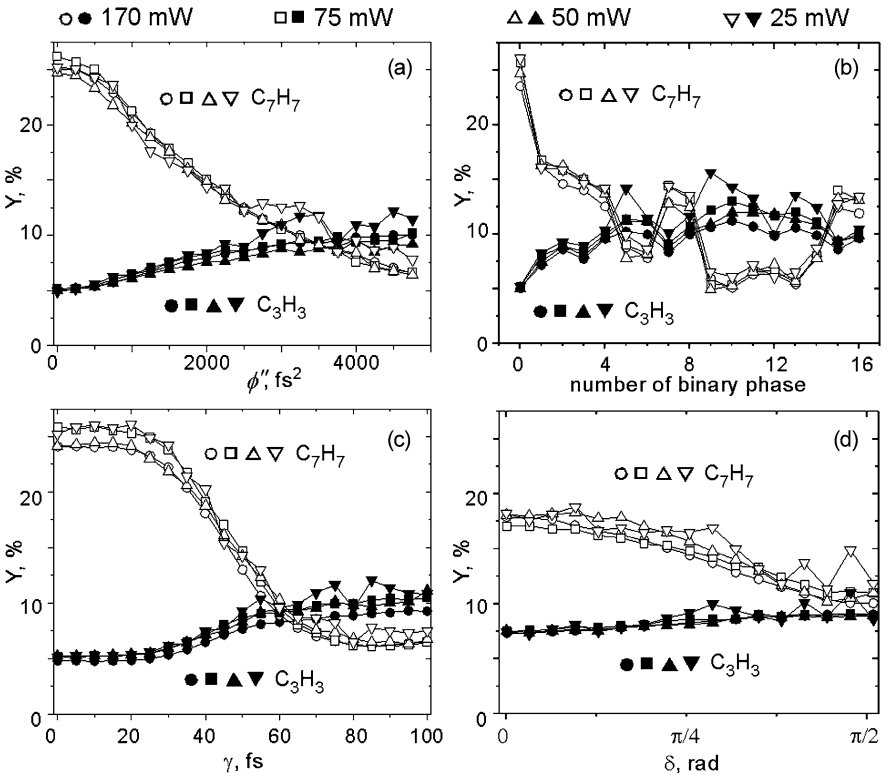

Fig. 8.10 [2] Percentage of total ionization measured at different laser powers (*dot*, *squares*, and *up* and *down triangle* for 170, 75, 50, and 25 μJ/pulse, respectively) for two main fragments of the dissociation of para-nitrotoluene, C_7H_7 (*open symbols*) and C_3H_3 (*filled symbols*), as a function of different methods of phase modulation, including (**a**) quadratic phase modulation, (**b**) 8-bit binary phase modulation, (**c**) sinusoidal phase modulation, as a function of modulation period, and (**d**) sinusoidal phase modulation as a function of phase factor. The difference of the signal for different powers is no more than the standard deviation of the measurements

to identify the most likely sites for photoionization. Further analysis of the fs-LID MS/MS spectra of a series of small peptides leads to the identification of principle cleavage pathways as well as some of the finer details of peptide dissociation by fs-LID.

8.4.1 Amino Acids

The fragmentation reactions of the protonated α-amino acids by CID have been described in detail, with dominant product ions corresponding to losses of NH_3, H_2O, and $H_2O + CO$ [93]. Fs-LID does not induce these same small molecule losses. Without derivatization, the only protonated amino acids that give rise to an fs-

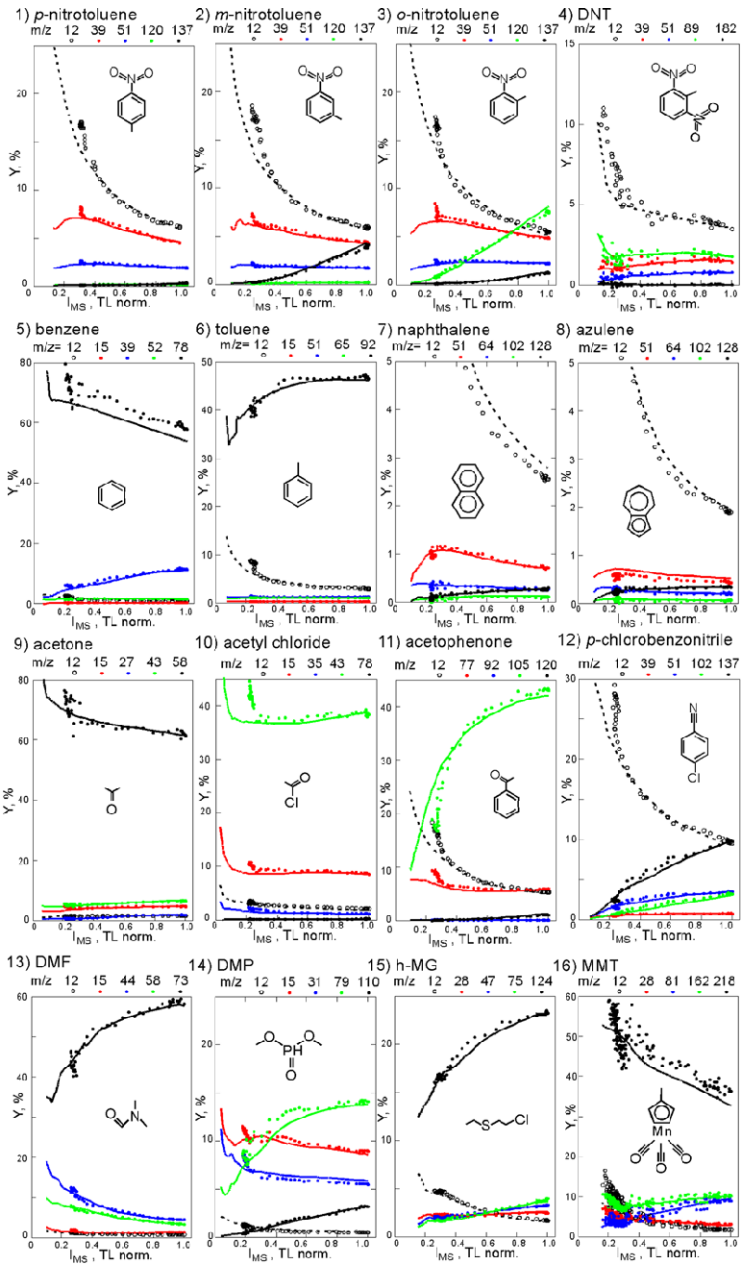

Fig. 8.11 [2] (1–16) Relative intensity of the most prominent ion products (Y), including C^+ (*open black*) and the molecular ion (*black dot*) as a function of the total yield of all ions (I_{MS}) for 16 different molecules as a function of linear chirp when the phase is scanned from 0 to 10,000 fs^2 (*lines*) and as a function of a sinusoidal phase modulation, where the period is scanned from 0 to 100 fs (*points*). Note the remarkable agreement between the two completely different types of phase modulation

Table 8.1 [5] The presence (Yes) or absence (No) of fs-LID signal is designated for each amino acid in the protonated $[M + H]^+$ form as well as the N-benzoyl and N-acetyl methyl ester derivatives. The calculated vertical ionization energies for several of the neutral amino acids in their low-lying conformations are reported [94] and experimental values from the NIST Chemistry Webbook are reported where possible

Amino Acid	IE of neutral (eV) [94]	$[M + H]^+$	N-benzoyl	N-acetyl methyl ester
A—Alanine	9.67 (NIST: 8.88)	No	No	No
C1—L-Cystine		No	No	Yes
C2—Cysteine	8.66 (NIST: 9–9.5)	No	No	Yes
D—Aspartic Acid	10.08	No	–	No
E—Glutamic Acid		No	No	No
F—Phenylalanine	8.40	Yes	Yes	Yes
G—Glycine	9.82 (NIST $\sim$ 9.2)	No	No	No
H—Histidine	7.76/8.34	No	No	No
I—Isoleucine	9.45 (NIST: 9.5)	No	No	Yes
K—Lysine	8.98 (NIST: 8.6–9.5)	No	No	Yes
L—Leucine	9.51 (NIST: 8.51)	No	Yes	Yes
M—Methionine	8.09 (NIST: 8.3–9.0)	Yes	Yes	Yes
N—Asparagine	9.31	No	Yes	No
P1—L-Proline	8.75 (NIST: 8.3–9.3)	No	Yes	Yes
P2—4-hydroxy-L-proline	(NIST: 9.1)	No	Yes	No
Q—Glutamine		No	No	No
R—Arginine	8.46	No	Yes	No
S—Serine	9.99 (NIST: 8.7–10)	No	Yes	No
T—Threonine	9.80 (NIST: < 10.2)	No	Yes	No
V—Valine	9.50 (NIST: 8.71)	No	No	No
W—Tryptophan	7.07 (NIST: < 7.5)	Yes	Yes	Yes
Y—Tyrosine	7.77 (NIST: < 8.4)	Yes	Yes	Yes

LID signal are methionine, phenylalanine, tryptophan, and tyrosine (see Table 8.1). These are the four amino acids with the lowest ionization energies, supporting the proposed photoionization mechanism for ion activation by fs-LID. However, ionization energy is not the sole predictor of fs-LID efficiency, as protonated phenylalanine gives rise to a more intense fs-LID signal than protonated methionine (data not shown) despite having a higher ionization energy. This suggests that polarizability of the precursor ions is critical to ion activation by fs-LID.

The CID and fs-LID MS/MS spectra for protonated tyrosine are compared in Fig. 8.12. As expected, the loss of NH_3 corresponds to the base peak observed in the CID spectrum, and $H_2O + CO$ losses are also observed. The same $H_2O + CO$ loss is observed following activation by fs-LID, but dissociation appears to proceed through the photoionized intermediate $[Y + H]^{2+\bullet}$, as confirmed by the MS^3 spec-

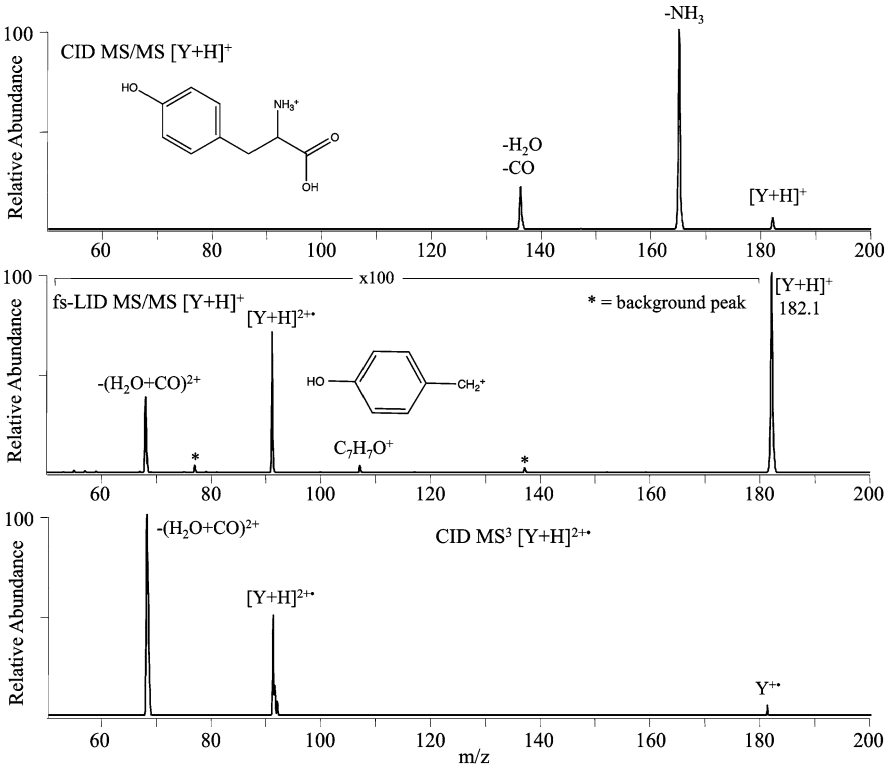

Fig. 8.12 [5] CID (*top*) and fs-LID (*middle*) spectra for protonated tyrosine illustrate the difference in dissociation pathways achieved by the two ion activation methods. CID MS^3 of the photoionization product (*lower* panel) indicates that $H_2O + CO$ loss proceeds through thermal excitation of the radical intermediate species

trum in the lower panel. NH_3 loss is absent in the fs-LID MS/MS spectrum and C_α–C_β bond dissociation gives rise to the $C_7H_7O^+$ product ion which was not observed by CID. Clearly, the two ion activation methods access different dissociation pathways.

Based on these results, which indicate that the presence of an aromatic ring enhances fs-LID activation, we evaluated all the amino acids after N-benzoyl derivatization. The presence of the benzoyl group led to a greater number of amino acids showing fs-LID ion activation events (see Table 8.1). The CID and fs-LID MS/MS spectra for N-benzoyl tyrosine are compared in Fig. 8.13. Once again, neutral losses dominate the CID spectrum while fs-LID ion activation proceeds through a radical intermediate. The photoionized $[BzY + H]^{2+\bullet}$ product ion is observed, as well as Bz^+ and $Y^{+\bullet}$, suggesting that the benzoyl group is a likely site of radical formation that leads to a radical-directed dissociation of the benzoyl group from the tyrosine molecule.

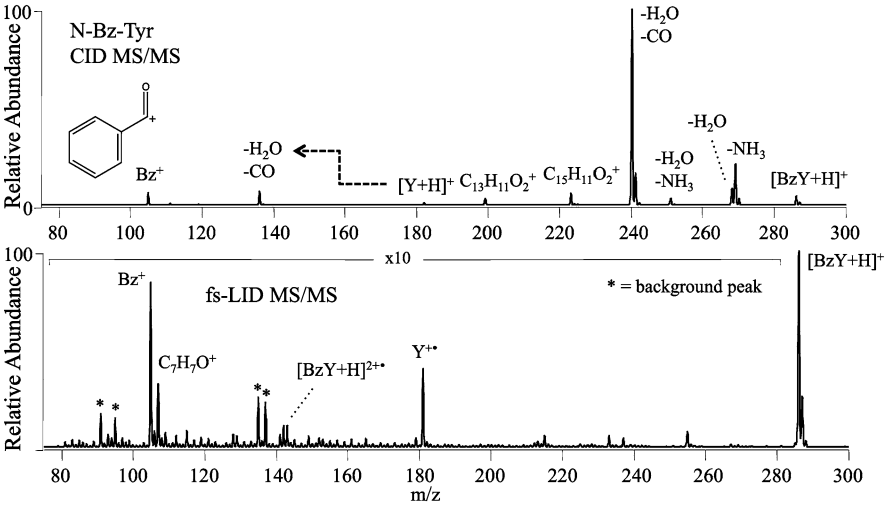

Fig. 8.13 [5] CID (*top*) and fs-LID (*bottom*) MS/MS spectra of N-benzoyl tyrosine. Note that NH_3 loss and minor product ions $C_{13}H_{11}O_2^+$ and $C_{15}H_{11}O_2^+$ in the CID spectrum indicate the presence of an isomeric impurity with the benzoyl addition occurring at the tyrosine side chain rather than the amine

We also evaluated N-acetyl methyl ester derivatized amino acids. This derivatization scheme was intended to simply lengthen each molecule, without the addition of a highly polarizable group. The CID and fs-LID MS/MS spectra for N-acetyl tyrosine methyl ester are shown in Fig. 8.14. The methyl ester and acetyl groups give rise to losses of CH_3OH, $CH_3OH + CO$, and CH_2CO following activation by CID, but these chemical modifications remain intact when ion activation is performed by fs-LID. The same $C_7H_7O^+$ fs-LID product ion is observed here as was seen for the other tyrosine-based precursors in Figs. 8.12 and 8.13.

Interestingly, between the two derivatization methods, we observed greater susceptibility to fs-LID for all amino acids except: alanine, aspartic acid, glutamic acid, glycine, histidine, glutamine and valine, as summarized in Table 8.1.

For a majority of the samples, the only product ion observed in the fs-LID MS/MS spectrum was the photoionization product, $[M + H]^{2+\bullet}$. However, the samples with the lowest ionization energies did demonstrate dissociation, primarily at the C_α–C_β bond. The series of spectra for the tyrosine samples provided in Figs. 8.12–8.14 are representative of the data for phenylalanine, methionine, and tryptophan. The photoionization product is observed in all three fs-LID MS/MS spectra, as is side chain product ion after cleavage of the C_α–C_β bond. Neutral losses of small molecules such as NH_3, H_2O, CO, CH_3OH, and CH_2CO dominate the CID spectra of these samples, but these thermal dissociation pathways are mitigated in fs-LID. These samples illustrate that fs-LID is complementary to CID, and that fs-LID spectra are rich in structural information, as the non-ergodic dissociation pathways lead to diagnostic product ions that are unique to the amino acid(s) in the

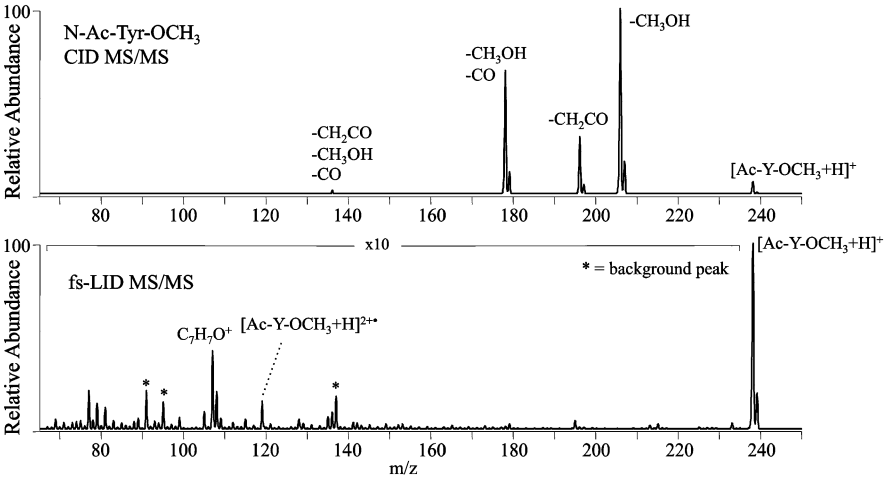

Fig. 8.14 [5] CID (*top*) and fs-LID (*bottom*) MS/MS spectra of the N-acetyl methyl ester tyrosine derivative

sample, rather than a series of small molecule losses that could be observed from any amino acid.

The fs-LID process is initiated by tunnel ionization of the most labile electron(s) in the molecule, and it leads to the formation of a radical cation. If no additional energy is deposited, the radical cation would fragment on a timescale long enough for intramolecular energy randomization leading to statistical bond breakage. Based on extensive experimental data, bond dissociation occurring in fs-LID is non-ergodic, suggesting that subsequent fragmentation occurs on a femtosecond timescale. We rationalize this by observing that the strong field acts on the entire macromolecule, pulling on most of the electrons. While usually only one electron is lost, one can assume that many other electrons are strongly perturbed by the field. This leads to energy being deposited on the macromolecule. This energy manifests as multiple bond breaking events recorded as a series of product ions for a particular peptide. The total energy deposited by the strong field on a typical singly protonated peptide can be estimated by adding the ionization energy (10.9 eV) [50] to the energy required to break one bond (4 eV) giving a total of $\sim$ 15 eV or $\sim$ 1450 kJ/mol. This amount of energy is equivalent to that of tens of photons and leads to ultrafast bond breaking. A more detailed analysis of the fs-LID process from single amino acids to peptides is given below.

8.4.2 Aromatics

Phenylalanine, tyrosine, and tryptophan all have ionization energies in the 7–8.5 eV range [94] and photoionize easily by fs-LID in both the protonated and derivatized

forms. While the delocalized pi systems stabilize the resulting radical, we do observe significant radical-directed cleavage of the C_α–C_β bonds in all three amino acids, giving rise to a singly charged product ion corresponding to the mass of the amino acid's side chain. The other major product in these fs-LID spectra is a doubly charged product ion that has lost neutral CO_2 from the carboxylic acid end of the molecule. Based on our observations, the aromatic amino acids are the most likely sites for radical formation when a peptide is subjected to fs-LID.

8.4.3 Acidic/Basic Amino Acids

Aspartic acid and glutamic acid show no ionization or dissociation into product ions via fs-LID, regardless of derivatization, which is consistent with their high ($\sim$ 10 eV) ionization energy. Histidine also gives rise to no fs-LID product ions, which is surprising given the low ($\sim$ 8 eV) estimated ionization energy of the neutral form. Most likely, protonation of the histidine side chain is interfering with the conjugated pi system of electrons, making them less polarizable and therefore less susceptible to strong field ionization.

Lysine and arginine show limited degrees of photoionization by fs-LID only after derivatization as an N-acetyl methyl ester and N-benzoyl derivative, respectively. Since the side chains of these residues are basic, they are probable sites of protonation, leaving few lone pair electrons susceptible to photoionization. Overall, the acidic and basic amino acids are unlikely origins for radical formation.

8.4.4 Polar Amino Acids

Glycine does not photoionize in any form, which is not surprising given that the hydrogen atom side chain does not enhance the polarizability of the amino acid backbone. More surprisingly, glutamine and its derivatives showed no fs-LID product ions, while asparagine gave rise to a small signal as an N-benzoyl derivative, as did serine and threonine. While the interaction of the benzoyl group with the backbone of each amino acid and the resulting stereochemistry are unique, the aromatic group does increase the polarizability of some of these previously inactive polar amino acids to the point that fs-LID signal can be observed. The bulky benzoyl group did not improve the amenability of cystine or cysteine to fs-LID, but a simple lengthening of the backbone in the N-acetyl methyl ester forms was sufficient to observe limited photoionization.

8.4.5 Non-polar Amino Acids

The susceptibility to fs-LID of the non-polar amino acids was found to increase with size and therefore polarizability. Alanine and valine were completely inactive,

while leucine, isoleucine, and proline could be photoionized upon derivatization (see Table 8.1). Methionine is the exception in this category—the S heteroatom in the side chain significantly lowers the ionization energy and accordingly, the activated sample gives rise to strong fs-LID product ions in all protonated and derivatized forms.

The fs-LID MS/MS analysis of single amino acids allowed us to elucidate the most likely origin of the $[M + H]^{2+\bullet}$ ion-radical pair. Methioinine and the aromatic residues are the most amenable to photoionization. Extending to slightly larger molecular systems, the fs-LID product ion signal seems to track with ionization potential or polarizability. Utilizing the benzoyl group as a chromophore was one successful method for generating fs-LID product ions from previously inactive samples. However, this sort of wet chemistry is unnecessary if the analyte is sufficiently large. The N-acetyl methyl ester derivatives were studied to mimic the lengthening of the backbone in a longer peptide or protein, and this modification also led to the observation of fs-LID product ions from previously inactive amino acids. Our conclusion is that longer peptides will be largely amenable to interrogation by fs-LID regardless of their sequence, without the need for any derivatization prior to MS/MS analysis.

8.4.6 Protein Sequencing

In proteomic MS/MS, the greater the number of assignable product ions observed, the more information-rich the spectrum can be considered. Peptide sequencing can be done manually or with the aid of software, whereby pairs of peaks that differ by the mass of a single amino acid are used to map out the identity and order of residues in the precursor sequence. If a specific region of the peptide does not fragment well, the exact sequence in that cannot be assigned. While some of the product ions corresponding to backbone cleavages may be redundant (in that we observe multiple cleavages between the same pair of residues), they increase our confidence in the ultimate sequence assignment. Therefore, it is advantageous to find an ion activation method that yields a greater variety of product ions, rather than simply a high intensity of product ions.

The robustness of fs-LID as an ion activation method is confirmed by the fs-LID spectrum of the peptide GAILAGAILA, which contains no aromatic or methionine residues (Fig. 8.15). The polarizability of the large molecule is sufficient for photoionization and gives rise to sufficient product ions for nearly 100 % sequence coverage. The most abundant product ions are the $-56^{2+\bullet}$ (side chain loss from Leu or Ile) and a nearly complete series of b-ions, limited only by the low mass cutoff (LMCO) associated with isolation of the precursor at 869.4 Da.

A single residue substitution at the C-terminal end of the peptide from alanine to arginine leads to a ∼7 % increase in dissociation efficiency by fs-LID (see Table 8.2) and also gives rise to more abundant a-ions near the C-terminal end of the

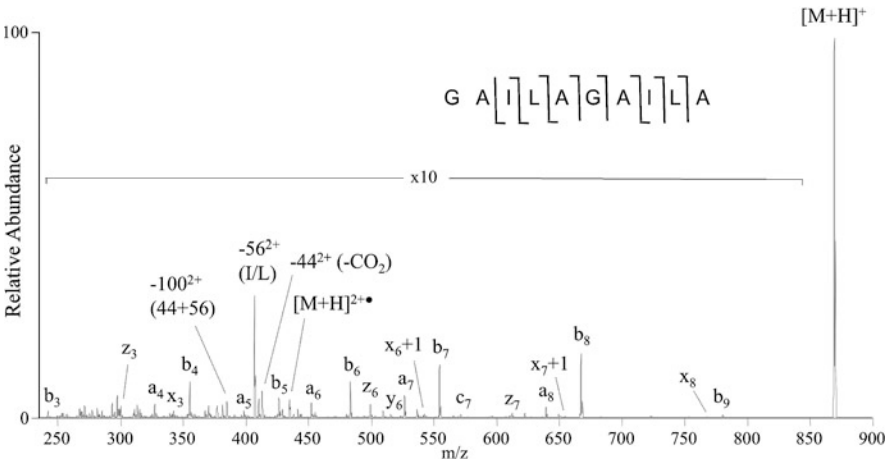

Fig. 8.15 [5] Fs-LID MS/MS spectrum for GAILAGAILA

Table 8.2 [5] Observed fs-LID dissociation efficiencies for a series of 12 synthetic peptides with sequence GAIL(X1)GAIL(X2). Efficiencies were calculated from the ratio of precursor ion abundances (normalized by the total ion current) in isolation and fs-LID spectra for each sample. Spectra for the three shaded samples can be found in Figs. 8.15–8.17

X1/**X2**	A	C	D	M
A	18.4 %	22.0 %	22.7 %	23.1 %
K	22.6 %	23.7 %	29.8 %	31.4 %
R	25.8 %	30.9 %	33.5 %	39.8 %

GAILAGAILR peptide (Fig. 8.16). This suggests that photoionization of the precursor occurs predominantly at the arginine residue. The -72^{2+} product ion corresponds to partial loss of the arginine side chain as a radical following cleavage of the C_β–C_γ bond while the rest of the peptide remains intact. Another notable feature in the fs-LID spectrum is the presence of satellite ions v_3, w_{b3}, w_{a7}, v_8, and w_{a8}, which can be used to differentiate between Ile and Leu residues when sequencing the peptide.

Alternatively, we can seed a likely origin for the radical into the peptide with a single residue substitution that places a methionine residue in the 5th position. This dramatically increases the fs-LID dissociation efficiency to nearly 40 % as shown in Table 8.2. This was expected given the fs-LID activity of protonated methionine observed earlier. Note that the fs-LID spectrum of GAILMGAILR (Fig. 8.17) has a base peak of $[M+H]^{2+\bullet}$ due to the stability of the radical formed at the methionine residue. This stability detracts slightly from the abundance of sequence ions, but also gives rise to strong side chain losses from methionine, -61^{2+} and $-74^{2+\bullet}$, that can be used as diagnostic indicators of methionine in unknown peptide or protein samples.

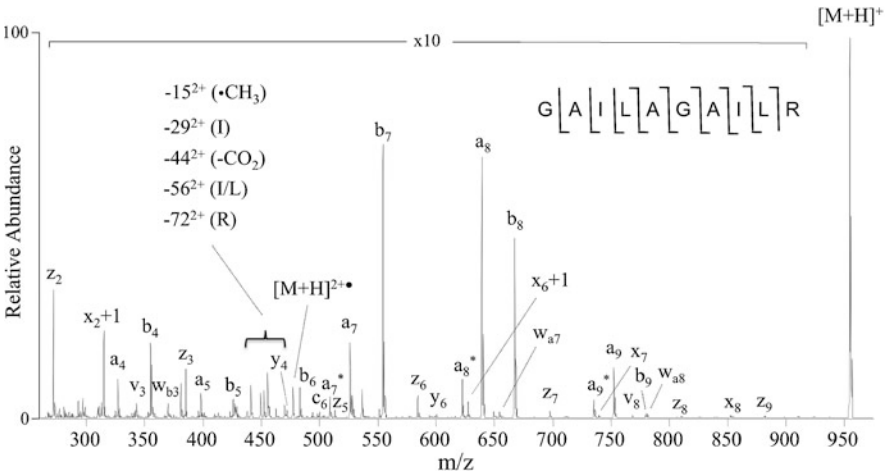

Fig. 8.16 [5] Fs-LID MS/MS spectrum for GAILAGAILR

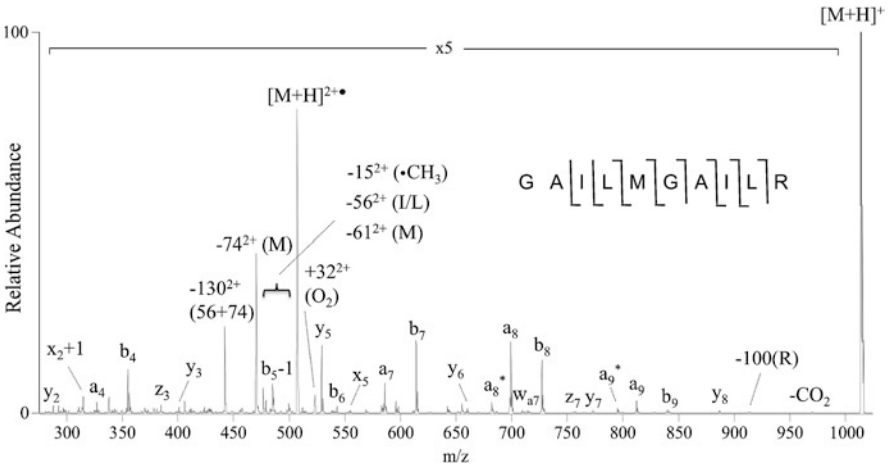

Fig. 8.17 [5] Fs-LID MS/MS spectrum for GAILMGAILR

The diagnostic side chain losses observed in fs-LID spectra of 12 synthetic peptides have been tabulated in Table 8.3 and are consistent with those reported in the literature [77, 78, 95]. Note that the neutral loss of even-electron species leaves a radical on the doubly charged peptide backbone, and can give rise to sequence ions, meaning that many of the side chain losses observed in fs-LID are intermediate rather than "dead-end" product ions. This opens the door for sequential dissociation, and also provides radical intermediates that can be isolated and subjected to MS^3 (or MS^n) for further analysis when present in sufficient abundance. The side chain losses from I, L, M, and R can be seen in the fs-LID spectra as noted in Figs. 8.15–8.17.

Table 8.3 [5] Observed fs-LID side chain losses from residues in the GAIL(X1)GAIL(X2) series

Residue	Mass of side chain loss (Da)	Chemical Formula
C	33	SH
D	44	CO_2
I	29, 56 (see Figs. 8.15–8.17)	$^{\bullet}C_2H_5$, C_4H_8
K	72	$^{\bullet}C_4H_{10}N$
L	43, 56 (see Figs. 8.15–8.17)	$^{\bullet}C_3H_7$, C_4H_8
M	61, 74 (see Figs. 8.17)	$^{\bullet}C_2H_5S$, C_3H_6S
R	72, 100 (see Figs. 8.16–8.17)	$^{\bullet}C_2H_6N_3$, $C_4H_{10}N_3^+$

The fs-LID dissociation efficiencies for the three peptide samples discussed above are combined with those of nine similar samples in Table 8.2. The peptide sequence is GAIL(X1)GAIL(X2) where X1 = alanine (A), cysteine (C), aspartic acid (D), or methionine (M) and X2 = alanine (A), lysine (K), or arginine (R). A two-way ANOVA test revealed that both the X1 effect and the X2 effect are statistically significant ($p = 0.0129$ and 0.0016, respectively). As the X1 residue changes from A to C to D to M, the polarizability of the peptide increases. As X2 changes from A to K to R, the proton mobility of the peptide decreases. Polarizability and proton mobility are not completely independent nor easily quantifiable for these samples, so the interaction effects cannot be analyzed.

In general, if the peptide being analyzed contains one or more F, M, W, or Y residues, we expect to see the photoionized $[M + H]^{2+\bullet}$ product as the base peak in the fs-LID MS/MS spectrum. In most other samples analyzed, products arising from side chain losses or sequence ions of type a and b are the most abundant, and all spectra contained a, b, x, y, and z-type ions. C-type sequence ions are the only product ions we do not observe regularly when using fs-LID for ion activation of these peptides. We also see an increase in sequence ion abundances near residues like C, K, and R, which have moderate ionization energies and are potential sites for side chain losses.

8.4.7 Bond Cleavage Pathways

Stabilization of the radical formed by photoionization can occur through H^+ or $H^{\bullet}$ abstraction. If the hydrogen atom comes from a side chain, the result is either a side chain loss, or propagation of the radical along the peptide chain. $H^{\bullet}$ transfer to a carbonyl along the peptide backbone as well as proton-driven chemistry will occur at the same time to produce sequence ions. A possible mechanism for each case is outlined in Fig. 8.18, where the ILM portion of the GAILMGAILR peptide is shown after undergoing photoionization. The radical is shown at its most likely origin, the S atom of the methionine side chain. Pathway (a) illustrates a potential $H^{\bullet}$ transfer which leads to migration of the radical two side chains down the peptide backbone to the C_β atom on the isoleucine side chain. This intermediate would

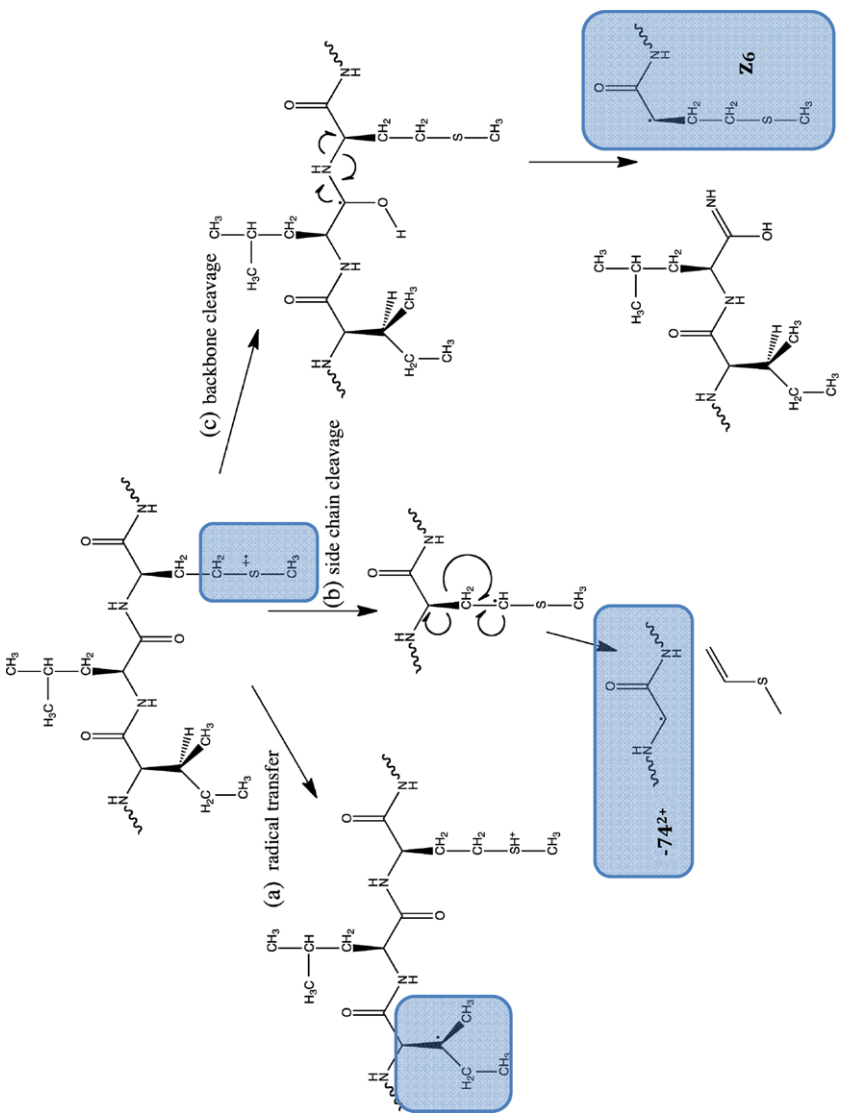

Fig. 8.18 [5] In the gas phase, the distonic species can dissociate via a number of pathways. The mechanisms shown here are meant to illustrate the variety of product ions that can form

then contribute to the -56^{2+} product ion abundance observed in Fig. 8.17. Pathway (b) follows the radical-directed cleavage of the C_α–C_β bond in the methionine side chain, resulting in the neutral loss of 74 Da, corresponding to the -74^{2+} product ion peak in Fig. 8.17. Finally, Pathway (c) illustrates one possible outcome of the radical migrating away from the methionine side-chain. The ion can now undergo a radical-directed backbone cleavage of the N–C_α bond in the peptide, resulting in c and/or z-type ions. Note that this mechanism is non-specific and could occur at various points along the peptide, giving rise to the z_3 and z_7 ions observed in Fig. 8.17. The mechanism is shown at the methionine residue here only for simplicity, in reality the resulting z_6 ion is a minor product ion and is not labeled in Fig. 8.17.

8.5 Discussion and Future Outlook

The ease with which femtosecond lasers are able to cause tunnel ionization in large isolated molecules and ions has led to the development of tools that have application in analytical chemistry. Already, fs-LID has been shown to generate information-rich MS/MS spectra. Through the analysis of protonated amino acids, we have identified the aromatic amino acids and methionine as the most likely sites of radical formation upon tunnel ionization, and have determined that ionization energy is not the sole predictor of sample amenability to fs-LID. As the fs-LID MS/MS spectra of the peptides illustrate, high polarizability and low proton mobility can boost fs-LID dissociation efficiency up above 35 %, even in samples with no aromatic chromophore to enhance ion activation. This makes fs-LID an attractive ion activation technique because it requires no chromophore or sample derivatization prior to MS/MS analysis. While a VUV laser can be used to efficiently photodissociate peptides due to the absorption maximum of peptide bonds around 190 nm [96], a femtosecond laser can activate any class of molecules via tunneling ionization, independent of their absorption spectra.

Another benefit of using femtosecond laser pulses is their ability to open several non-ergodic dissociation pathways, wherein stronger bonds are broken and more labile bonds remain intact. This observation has lead to a number of fundamental studies, and is a major attraction as an analytical tool. In particular, non-ergodic dissociation is valuable for the analysis of post-translational modification. There is an alternative method for inducing this type of gas phase radical known as electron capture or electron transfer dissociation (ECD/ETD), which reduces multiply charged gas phase ions to form hydrogen-abundant radical cations ($[M + 2H]^{2+} \rightarrow [M + 2H]^{+\bullet}$). By comparison, fs-LID intermediates are hydrogen-deficient ($[M + H]^{+} \rightarrow [M + H]^{2+\bullet}$), and therefore the technique does not need a multiply charged precursor to carry out ion activation in positive ion mode. This makes fs-LID appropriate for pairing with laser desorption sources such as MALDI, as the soft ionization method is known to generate singly protonated ions. Preliminary studies in negative ion mode using fs-LID have also shown promising results and higher product ion yields, indicating that fs-LID may one day be appropriate for high throughput proteomic and metabolomic studies.

In conclusion, fundamental studies on the strong-field interaction between femtosecond lasers and large organic molecules has resulted in important analytical tools that may one day advance diverse fields such as drug discovery and medical diagnosis.

Acknowledgements The instrument used for the fs-LID work was funded by grant 156 of the 21st Century Jobs Trust Fund of the SEIC Board from the State of Michigan. Additional support comes from grant CRIF ID 0923957 from the National Science Foundation. The results presented here would not be available without the work of very talented colleagues. We specifically thank Professors Gavin E. Reid and A. Daniel Jones who collaborated in the initial development of the fs-LID method. We are also thankful for the careful and persistent work on the effects of pulse shaping on molecular fragmentation by Xin Zhu, and the analysis and suggestion of multiple experiments by Dr. Vadim V. Lozovoy,

References

1. J.H. Posthumus, Rep. Prog. Phys. **67**, 623 (2004)
2. V.V. Lozovoy, X. Zhu, T.C. Gunaratne, D.A. Harris, J.C. Shane, M. Dantus, J. Phys. Chem. A **112**, 3789 (2008)
3. S.M. Hankin, D.M. Villeneuve, P.B. Corkum, D.M. Rayner, Phys. Rev. A **64** (2001)
4. C. Uiterwaal, C.R. Gebhardt, H. Schroder, K.L. Kompa, Eur. Phys. J. D **30**, 379 (2004)
5. C.L. Kalcic, G.E. Reid, V.V. Lozovoy, M. Dantus, J. Phys. Chem. A (2011)
6. E. Mevel, P. Breger, R. Trainham, G. Petite, P. Agostini, A. Migus, J.P. Chambaret, A. Antonetti, Phys. Rev. Lett. **70**, 406 (1993)
7. R.J. Levis, M.J. DeWitt, J. Phys. Chem. A **103**, 6493 (1999)
8. J.B. Fenn, M. Mann, C.K. Meng, S.F. Wong, C.M. Whitehouse, Science **246**, 64 (1989)
9. F. Hillenkamp, M. Karas, R.C. Beavis, B.T. Chait, Anal. Chem. **63**, A1193 (1991)
10. J.R. Yates, J. Mass Spectrom. **33**, 1 (1998)
11. L. Sleno, D.A. Volmer, J. Mass Spectrom. **39**, 1091 (2004)
12. V.H. Wysocki, K.A. Resing, Q.F. Zhang, G.L. Cheng, Methods **35**, 211 (2005)
13. A.H. Zewail, Phys. Today **33**, 27 (1980)
14. M. Dantus, M.J. Rosker, A.H. Zewail, J. Chem. Phys. **87**, 2395 (1987)
15. D.J. Tannor, S.A. Rice, J. Chem. Phys. **83**, 5013 (1985)
16. P. Brumer, M. Shapiro, Chem. Phys. Lett. **126**, 541 (1986)
17. D.J. Tannor, R. Kosloff, S.A. Rice, J. Chem. Phys. **85**, 5805 (1986)
18. J.L. Krause, R.M. Whitnell, K.R. Wilson, Y.J. Yan, S. Mukamel, J. Chem. Phys. **99**, 6562 (1993)
19. I. Pastirk, E.J. Brown, Q.G. Zhang, M. Dantus, J. Chem. Phys. **108**, 4375 (1998)
20. T. Brixner, G. Gerber, ChemPhysChem **4**, 418 (2003)
21. M. Dantus, V.V. Lozovoy, Chem. Rev. **104**, 1813 (2004)
22. A. Assion, T. Baumert, M. Bergt, T. Brixner, B. Kiefer, V. Seyfried, M. Strehle, G. Gerber, Science **282**, 919 (1998)
23. M. Bergt, T. Brixner, B. Kiefer, M. Strehle, G. Gerber, J. Phys. Chem. A **103**, 10381 (1999)
24. T. Brixner, B. Kiefer, G. Gerber, Chem. Phys. **267**, 241 (2001)
25. M. Bergt, T. Brixner, C. Dietl, B. Kiefer, G. Gerber, J. Organomet. Chem. **661**, 199 (2002)
26. T. Brixner, N.H. Damrauer, G. Krampert, P. Niklaus, G. Gerber, J. Mod. Opt. **50**, 539 (2003)
27. R.J. Levis, G.M. Menkir, H. Rabitz, Science **292**, 709 (2001)
28. R.J. Levis, H.A. Rabitz, J. Phys. Chem. A **106**, 6427 (2002)
29. P. Graham, G. Menkir, R.J. Levis, Spectrochim. Acta, Part B, At. Spectrosc. **58**, 1097 (2003)
30. C. Daniel, J. Full, L. Gonzalez, C. Kaposta, M. Krenz, C. Lupulescu, J. Manz, S. Minemoto, M. Oppel, P. Rosendo-Francisco, S. Vajda, L. Woste, Chem. Phys. **267**, 247 (2001)

31. C. Daniel, J. Full, L. Gonzalez, C. Lupulescu, J. Manz, A. Merli, S. Vajda, L. Woste, Science **299**, 536 (2003)
32. D. Cardoza, F. Langhojer, C. Trallero-Herrero, O.L.A. Monti, T. Weinacht, Phys. Rev. A **70** (2004)
33. F. Langhojer, D. Cardoza, M. Baertschy, T. Weinacht, J. Chem. Phys. **122** (2005)
34. D. Cardoza, M. Baertschy, T. Weinacht, J. Chem. Phys. **123** (2005)
35. D. Cardoza, C. Trallero-Herrero, F. Langhojer, H. Rabitz, T. Weinacht, J. Chem. Phys. **122** (2005)
36. D. Cardoza, B.J. Pearson, M. Baertschy, T. Weinacht, J. Photochem. Photobiol. A, Chem. **180**, 277 (2006)
37. D. Cardoza, M. Baertschy, T. Weinacht, Chem. Phys. Lett. **411**, 311 (2005)
38. E. Wells, K.J. Betsch, C.W.S. Conover, M.J. DeWitt, D. Pinkham, R.R. Jones, Phys. Rev. A **72** (2005)
39. R.S. Judson, H. Rabitz, Phys. Rev. Lett. **68**, 1500 (1992)
40. M. Wollenhaupt, A. Prakelt, C. Sarpe-Tudoran, D. Liese, T. Baumert, J. Opt. B, Quantum Semiclass. Opt. **7**, S270 (2005)
41. B.J. Sussman, D. Townsend, M.Y. Ivanov, A. Stolow, Science **314**, 278 (2006)
42. I. Pastirk, M. Kangas, M. Dantus, J. Phys. Chem. A **109**, 2413 (2005)
43. J.C. Shane, V.V. Lozovoy, M. Dantus, J. Phys. Chem. A **110**, 11388 (2006)
44. V.V. Lozovoy, M. Dantus, ChemPhysChem, **6**, 1970 (2005)
45. V.V. Lozovoy, T.C. Gunaratne, J.C. Shane, M. Dantus, ChemPhysChem **7**, 2471 (2006)
46. V.V. Lozovoy, M. Dantus, Annu. Rep. Prog. Chem., Sect. C, Phys. Chem. **102** (2006)
47. V.V. Lozovoy, I. Pastirk, M. Dantus, Opt. Lett. **29**, 775 (2004)
48. Y. Coello, V.V. Lozovoy, T.C. Gunaratne, B.W. Xu, I. Borukhovich, C.H. Tseng, T. Weinacht, M. Dantus, J. Opt. Soc. Am. B, Opt. Phys. **25**, A140 (2008)
49. C.L. Kalcic, T.C. Gunaratne, A.D. Jones, M. Dantus, G.E. Reid, J. Am. Chem. Soc. **131**, 940 (2009)
50. B.A. Budnik, Y.O. Tsybin, P. Hakansson, R.A. Zubarev, J. Mass Spectrom. **37**, 1141 (2002)
51. S.A. Smith, C.L. Kalcic, K.A. Safran, P.M. Stemmer, M. Dantus, G.E. Reid, J. Am. Soc. Mass Spectrom. **21**, 2031 (2010)
52. S.A. Smith, C.L. Kalcic, M. Dantus, G.E. Reid, Phospholipid analysis by femtosecond laser-induced ionization/dissociation mass spectrometry (fs-LID MS), in *57th ASMS Conference* (2009)
53. N.S. Winkler, C.L. Kalcic, A.D. Jones, M. Dantus, Study of metabolites including alpha-tomatine by femtosecond laser-induced ionization/dissociation (fs-LID), in *57th ASMS Conference* (2009)
54. X. Zhu, C.L. Kalcic, N. Winkler, V.V. Lozovoy, M. Dantus, J. Phys. Chem. A **114**, 10380 (2010)
55. A.R. Dongre, J.L. Jones, A. Somogyi, V.H. Wysocki, J. Am. Chem. Soc. **118**, 8365 (1996)
56. E.A. Kapp, F. Schütz, G.E. Reid, J.S. Eddes, R.L. Moritz, R.A. O'Hair, T.P. Speed, R.J. Simpson, J. Anal. Chem. **75**, 6251 (2003)
57. V.H. Wysocki, G. Tsaprailis, L.L. Smith, L.A. Breci, J. Mass Spectrom. **35**, 1399 (2000)
58. D. Pu, N.L. Clipston, C.J. Cassady, J. Mass Spectrom. **45**, 297 (2010)
59. J.J. Gorman, T.P. Wallis, J.J. Pitt, Mass Spectrom. Rev. **21**, 183 (2002)
60. A.M. Palumbo, J.J. Tepe, G.E. Reid, J. Proteome Res. **7**, 771 (2008)
61. A.M. Palumbo, G.E. Reid, Anal. Chem. **80**, 9735 (2008)
62. R.A. Zubarev, D.M. Horn, E.K. Fridriksson, N.L. Kelleher, N.A. Kruger, M.A. Lewis, B.K. Carpenter, F.W. McLafferty, Anal. Chem. **72**, 563 (2000)
63. L.M. Mikesh, B. Ueberheide, A. Chi, J.J. Coon, J.E.P. Syka, J. Shabanowitz, D.F. Hunt, Biochim. Biophys. Acta, Proteins Proteomics **1764**, 1811 (2006)
64. J. Wiesner, T. Premsler, A. Sickmann, Proteomics **8**, 4466 (2008)
65. J.J. Wilson, J.S. Brodbelt, Anal. Chem. **79**, 7883 (2007)
66. J.J. Wilson, G.J. Kirkovits, J.L. Sessler, J.S. Brodbelt, J. Am. Soc. Mass Spectrom. **19**, 257 (2008)

67. L. Joly, R. Antoine, M. Broyer, P. Dugourd, J. Lemoine, J. Mass Spectrom. **42**, 818 (2007)
68. S.H. Yoon, Y.J. Chung, M.S. Kim, J. Am. Soc. Mass Spectrom. **19**, 645 (2008)
69. M. Perot, B. Lucas, M. Barat, J.A. Fayeton, C. Jouvet, J. Phys. Chem. A **114**, 3147 (2010)
70. T.Y. Kim, J.P. Reilly, J. Am. Soc. Mass Spectrom. **20**, 2334 (2009)
71. R. Parthasarathi, Y. He, J.P. Reilly, K. Raghavachari, J. Am. Chem. Soc. **132**, 1606 (2010)
72. J.A. Madsen, D.R. Boutz, J.S. Brodbelt, J. Proteome Res. **9**, 4205 (2010)
73. J.A. Madsen, T.S. Kaoud, K.N. Dalby, J.S. Brodbelt, Proteomics **11**, 1329 (2011)
74. W.D. Cui, M.S. Thompson, J.P. Reilly, J. Am. Soc. Mass Spectrom. **16**, 1384 (2005)
75. J.P. Reilly, Mass Spectrom. Rev. **28**, 425 (2009)
76. B.N. Moore, S.J. Blanksby, R.R. Julian, Chem. Commun. **5015** (2009)
77. Q.Y. Sun, H. Nelson, T. Ly, B.M. Stoltz, R.R. Julian, J. Proteome Res. **8**, 958 (2009)
78. M.M. Savitski, M.L. Nielsen, R.A. Zubarev, Anal. Chem. **79**, 2296 (2007)
79. W.H. Renninger, A. Chong, F.W. Wise, Phys. Rev. A **82** (2010)
80. B. Nie, D. Pestov, F.W. Wise, M. Dantus, Opt. Express **19**, 12074 (2011)
81. W.J. Jia, K.W.D. Ledingham, C.T.J. Scott, C. Kosmidis, R.P. Singhal, Rapid Commun. Mass Spectrom. **10**, 1597 (1996)
82. T. Laarmann, I. Shchatsinin, P. Singh, N. Zhavoronkov, M. Gerhards, C.P. Schulz, I.V. Hertel, J. Chem. Phys. **127** (2007)
83. L. Guyon, T. Tabarin, B. Thuillier, R. Antoine, M. Broyer, V. Boutou, J.P. Wolf, P. Dugourd, J. Chem. Phys. **128** (2008)
84. H. Kang, C. Jouvet, C. Dedonder-Lardeux, S. Martrenchard, G. Gregoire, C. Desfrancois, J.P. Schermann, M. Barat, J.A. Fayeton, Phys. Chem. Chem. Phys. **7**, 394 (2005)
85. G. Gregoire, H. Kang, C. Dedonder-Lardeux, C. Jouvet, C. Desfrancois, D. Onidas, V. Lepere, J.A. Fayeton, Phys. Chem. Chem. Phys. **8**, 122 (2006)
86. T. Ergler, A. Rudenko, B. Feuerstein, K. Zrost, C.D. Schroter, R. Moshammer, J. Ullrich, Phys. Rev. Lett. **97** (2006)
87. W.A. Bryan, J. McKenna, E.M.L. English, J. Wood, C.R. Calvert, R. Torres, D.S. Murphy, I.C.E. Turcu, J.L. Collier, J.F. McCann, I.D. Williams, W.R. Newell, Phys. Rev. A **76** (2007)
88. S. De, M. Magrakvelidze, I.A. Bocharova, D. Ray, W. Cao, I. Znakovskaya, H. Li, Z. Wang, G. Laurent, U. Thumm, M.F. Kling, I.V. Litvinyuk, I. Ben-Itzhak, C.L. Cocke, Phys. Rev. A **84** (2011)
89. X. Zhu, V.V. Lozovoy, J.D. Shah, M. Dantus, J. Phys. Chem. A **115**, 1305 (2011)
90. S.M. Hankin, D.M. Villeneuve, P.B. Corkum, D.M. Rayner, Phys. Rev. Lett. **84**, 5082 (2000)
91. D.B. Galloway, J.A. Bartz, L.G. Huey, F.F. Crim, J. Chem. Phys. **98**, 2107 (1993)
92. P. Lablanquie, K. Ohashi, N. Nishi, J. Chem. Phys. **98**, 399 (1993)
93. N.N. Dookeran, T. Yalcin, A.G. Harrison, J. Mass Spectrom. **31**, 500 (1996)
94. D. Dehareng, G. Dive, Int. J. Mol. Sci. **5**, 301 (2004)
95. J. Laskin, Z.B. Yang, C.M.D. Ng, I.K. Chu, J. Am. Soc. Mass Spectrom. **21**, 511 (2010)
96. A.R. Goldfarb, L.J. Saidel, E. Mosovich, J. Biol. Chem. **193**, 397 (1951)